Global and Planetary Change 115 (2014) 44–58

Contents lists available at ScienceDirect

Global and Planetary Change

journal homepage: www.elsevier.com/locate/gloplacha

Global suspended sediment and water discharge dynamics between 1960 and 2010: Continental trends and intra-basin sensitivity

Sagy Cohen [a,*], Albert J. Kettner [b], James P.M. Syvitski [b]

[a] Department of Geography, University of Alabama, Box 870322, Tuscaloosa, AL 35487, USA
[b] Community Surface Dynamics Modeling System, Institute of Arctic and Alpine Research, University of Colorado, Boulder, CO 80309, USA

ARTICLE INFO

Article history:
Received 12 September 2012
Received in revised form 18 January 2014
Accepted 22 January 2014
Available online 29 January 2014

Keywords:
suspended sediment
water discharge
global
modeling
rivers

ABSTRACT

Establishing a quantitative description of global riverine fluxes is one of the main goals of contemporary hydrology and geomorphology. Here we study changes in global riverine water discharge and suspended sediment flux over a 50-year period, 1960–2010, applying a new version of the WBMsed (WBMsed v.2.0) global hydrological water balance model. A new floodplain component is introduced to better represent water and sediment dynamics during periods of overbank discharge. Validated against data from 16 globally distributed stations, WBMsed v.2.0 simulation results show considerable improvement over the original model. Normalized departure from an annual mean is used to quantify spatial and temporal dynamics in both water discharge and sediment flux. Considerable intra-basin variability in both water and sediment discharge is observed for the first time in different regions of the world. Continental-scale analysis shows considerable variability in water and sediment discharge fluctuations both in time and between continents. A correlation analysis between predicted continental suspended sediment and water discharge shows strong correspondence in Australia and Africa (R^2 of 0.93 and 0.87 respectively), moderate correlation in North and South America (R^2 of 0.64 and 0.73 respectively) and weak correlation in Asia and Europe (R^2 of 0.35 and 0.24 respectively). We propose that yearly changes in intra-basin precipitation dynamics explain most of these differences in continental water discharge and suspended sediment correlation. The mechanism proposed and demonstrated here (for the Ganges, Danube and Amazon Rivers) is that regions with high relief and soft lithology will amplify the effect of higher than average precipitation by producing an increase in sediment yield that greatly exceeds increase in water discharge.

1. Introduction

Quantifying riverine sediment flux and water discharge is an important scientific undertaking for many reasons. Water discharge is a key component in the global water cycle affecting our planet's climate (Harding et al., 2011), ecology (Doll et al., 2009) and anthropogenic activities (e.g. agriculture, drinking water, recreation; Biemans et al., 2011). Quantifying sediment flux dynamics is a fundamental goal of earth-system science for its role in our planet's geology (Pelletier, 2012), biogeochemistry (Vörösmarty et al., 1997; Syvitski and Milliman, 2007) and anthropogenic activities (Kettner et al., 2010). Our quantitative understanding and predictive capabilities of global river fluxes are lacking (Harding et al., 2011). This is, in part, due to the multi-scale nature of the processes involved (Pelletier, 2012) and the inadequacy in global gauging of rivers (Fekete and Vörösmarty, 2007). Availability of measured river fluxes is decreasing globally (Brakenridge et al., 2012) particularly for sediment (Syvitski et al., 2005). Sediment fluxes to the oceans are measured for less than 10% of the Earth's rivers (Syvitski et al., 2005) and intra-basin measurements are even scarcer (Kettner et al., 2010).

Numerical models can fill the gap in sediment measurements (e.g. Syvitski et al., 2005; Wilkinson et al., 2009) and offer predictive or analytical capabilities of future and past trends enabling the investigations of terrestrial response to environmental and human changes (e.g. climate change; Kettner and Syvitski, 2009). Despite advances made in recent years (e.g. Kettner and Syvitski, 2008; Pelletier, 2012; Cohen et al., 2013) simulating global riverine fluxes remains challenging.

Climate change during the 21st century is projected to alter the spatio-temporal dynamics of precipitation and temperature (Held and Soden, 2006; Bates et al., 2008) resulting in natural and anthropogenically induced changes in land-use and water availability (Bates et al., 2008). Estimating the effect of these spatially and temporally dynamic processes warrants sophisticated distributed numerical models. Using past trends is perhaps the best strategy for developing these models and improving our understanding of the dynamics and causality within these complex systems.

Herein we present and validate an improved version of the WBMsed global riverine sediment flux model (Cohen et al., 2013). Cohen et al. (2013) showed that WBMsed can capture long-term average and inter-annual suspended sediment fluxes but tends to overestimate daily fluxes (by orders of magnitudes) during high discharge events and underestimate these during low flow periods. We found that these sediment flux miss-predictions are directly linked to miss-

* Corresponding author. Tel.: 1 205 348 5860; fax: 1 205 348 2278.
E-mail address: sagy.cohen@ua.edu (S. Cohen).

0921-8181/$ – see front matter © 2014 Elsevier B.V. All rights reserved.
http://dx.doi.org/10.1016/j.gloplacha.2014.01.011

predictions of riverine water discharge, as the model's water routing approach did not limit the water transfer capacity of rivers. In other words, the model did not consider overbank flow and water storage in floodplains. For a natural river system, flooding not only limits the amount of water that can be transported over a certain period of time by a river but also provides a temporary reservoir that will resupply water back to the river days after the flood. The absence of such mechanism will result in a modeled river system that is overly responsive to runoff (i.e. overestimation during peak flow and underestimation during low flows) (Coe et al., 2008; Paiva et al., 2011; Yamazaki et al., 2011). Here we employ a floodplain reservoir component to store overbank flow at a pixel scale resulting in more realistic riverine flux predictions during peak and low flow conditions.

The new model is used to simulate water discharge and suspended sediment flux (at 6 arc-minute resolution) between 1960 and 2010. The results are used to analyze the yearly trends (normalized departure from mean) at both pixel scale and continental average. In this paper we focus our analysis on continental-scale interplay between suspended sediment flux and water discharge. A more focused analysis in three large basins (Ganges, Danube and Amazon) is preformed to explain discrepancies between water and sediment discharge, demonstrating an intriguing spatial–temporal interplay between lithology, topography and precipitation.

2. Methodology

2.1. The WBMsed v.2.0 model

WBMsed is a fully distributed global suspended sediment flux model (Cohen et al., 2013). It is an extension of the WBMplus global hydrology model (Wisser et al., 2010), part of the FrAMES biogeochemical modeling framework (Wollheim et al., 2008).

2.1.1. Water discharge module

The WBMplus model includes the water balance/transport model first introduced by Vörösmarty et al. (1989) and subsequently modified by Wisser et al. (2010). At its core the surface water balance of non-irrigated areas is a simple soil moisture budget expressed as:

$$dW_s/dt = \begin{cases} -g(W_s)\left(E_p - P_a\right) & P_a \le E_p \\ P_a - E_p & E_p < P_a \le D_{ws} \\ D_{ws} - E_p & D_{ws} < P_a \end{cases} \quad (1)$$

driven by $g(W_s)$, a dimensionless soil function:

$$g(W_s) = \frac{1 - e^{\left(-\alpha \frac{W_s}{W_c}\right)}}{1 - e^{-\alpha}} \quad (2)$$

where W_s is soil moisture, E_p is potential evapotranspiration, P_a is precipitation (rainfall P_r combined with snowmelt M_s), and D_{ws} is soil moisture deficit. Soil moisture deficit is the difference between available water capacity (W_c) and soil moisture. Available water capacity is dependent on soil and vegetation characteristics of each grid-cell (specified by input layers). The dimensionless empirical constant α is set to 5.0 following Vörösmarty et al. (1989).

Flow routing from grid to grid cell follows a downstream grid-cell tree topology (that allows the conjunctions of grid cells upstream but does not include diversions to, for example, river channel bars or multiple distributary channel deltas). Implementation uses the Muskingum–Cunge equation, a semi-implicit finite difference scheme to provide the diffusive wave solution to the St. Venant equations (ignoring the two acceleration terms in the momentum equation). The Muskingum–Cunge method is not the full-implementation of the diffusive wave approximation of the St. Venant equation. The Muskingum–Cunge solution includes a local diffusive effect within a single grid-cell, however it does not represent the diffusive effect between upstream and downstream grid-cells. Thus, the backwater effect caused by the water level rise in the downstream grid-cell is not represented in the calculation of the upstream discharge.

The equation is expressed as a linear combination of the input flow from current and previous time steps ($Q_{in\ t-1}$, $Q_{in\ t}$) and the released water from the river segment (grid-cell) in the previous time step ($Q_{out\ t-1}$) to calculate the new grid-cell outflow ($Q_{out\ t}$):

$$Q_{out\,t} = c_1 Q_{in\,t} + c_2 Q_{in\,t-1} + c_3 Q_{out\,t-1}. \quad (3)$$

The Muskingum coefficients (c_1, c_2, c_3) are traditionally estimated experimentally from discharge records, but their relationships to channel properties are well established. Detailed descriptions are provided in Wisser et al. (2010).

The new floodplain reservoir module (Fig. 1) adjusts daily water discharge for each grid-cell based on its bankfull discharge. When predicted water discharge ($Q_{out\ t}$) exceeds bankfull discharge (Q_{bf}) the "excess" water ($Q_{out\ t} - Q_{bf}$) will be stored in a virtual infinite floodplain reservoir and the new streamflow will equal bankfull discharge ($Q_{out\,t} = Q_{bf}$) (Fig. 1a). It should be noted that riverine water discharge cannot realistically exceed bankfull discharge and so the described equations below are an algorithmic rather than a physically-based solution. Once predicted water discharge is below bankfull again, water held in the floodplain reservoir will be reinjected to the river grid-cell. The volume of water returning to the river in a given time-step is proportional to the river grid-cell deficit from bankfull ($Q_{bf} - Q_{out\ t}$), i.e. very low river flows will result in greater reinjection of floodplain water (Fig. 1b). The changes in water discharge can be formulated as:

$$Q_{out\_aj} = \begin{cases} Q_{bf} & Q_{out\_t} > Q_{bf} \\ Q_{out\_t} + \left(Q_{bf} - Q_{out\_t}\right) b & Q_{out\_t} < Q_{bf} \end{cases} \quad (4)$$

where Q_{out_aj} is the adjusted river water discharge (m^3/s) and b is a daily delay fraction of water flow from the floodplain to the river ($b = 1$ translates to no delay (open flow)). For simplicity we assume here that $b = 1$ however a more complex description of b can be employed.

Bankfull discharge at a river segment is estimated using an approach modified from the river morphology module in the CaMa-Flood model (Yamazaki et al., 2011)

$$Q_{bf} = HWV_{bf} \quad (5)$$

where H is bank height

$$H = \mathrm{Max}\left[0.5\overline{Q}^{0.3}, 1.0\right] \quad (6)$$

where $\overline{Q}$ is long term average discharge, W is channel width

$$W = \mathrm{Max}\left[15\overline{Q}^{0.5}, 10.0\right] \quad (7)$$

and V_{bf} is bankfull flow velocity

$$V_{bf} = n^{-1} S^{-1/2} H^{2/3} \quad (8)$$

where n is Manning's roughness coefficient (0.03) and S, slope (m/m), is assumed to be constant. Here we used a slope value of 0.001 as a midpoint between very large, low-gradient rivers (e.g. Mississippi and Amazon with a slope of about 2.0×10^{-5}; Nittrouer et al., 2008 and LeFavour and Alsdorf, 2005) and steep headwater rivers (with gradients greater than 0.1; Chiari et al., 2010). A spatially explicit riverine slope description will improve the accuracy of this algorithm and is currently under development.

Additional approaches for estimating bankfull discharge were extensively tested. We have found that the Pearson III flood frequency estimator (using a 5-year flood frequency parameter) resulted in fairly realistic results. However this purely statistical methodology proved to

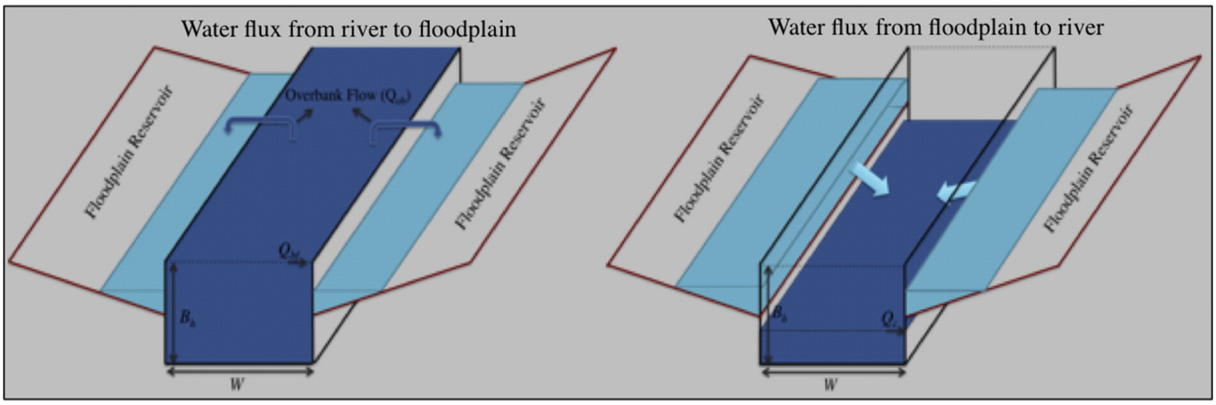

Fig. 1. Schematics of the WBMsed v.2.0 floodplain reservoir component. After Yamazaki et al. (2011).

be inferior to the methodology presented above for larger rivers and was therefore discarded.

2.1.2. Sediment flux module

Similar to the first version of the model (WBMsed; Cohen et al., 2013) the suspended sediment flux module is a spatially explicit implementation of the *BQART* and *Psi* basin outlet models (Syvitski and Milliman, 2007; Morehead et al., 2003 respectively). In order to simulate these models continuously in space (i.e. pixel-scale) we assume that each pixel is an outlet of its upstream contributing area (plus its own area). The *BQART* model simulate long-term (30+ years) average suspended sediment loads $\overline{Q_s}$ for a basin outlet

$$\overline{Q}_s = \omega B \overline{Q}^{0.3} A^{0.5} RT \text{ for } T \geq 2\ ^\circ\text{C}, \tag{9a}$$

$$\overline{Q}_s = 2\omega B \overline{Q}^{0.3} A^{0.5} RT \text{ for } T \geq 2\ ^\circ\text{C}, \tag{9b}$$

where ω is the coefficient of proportionality that equals 0.02 for units of kg s^{-1}, Q is long-term average discharge for each cell (m^3/s^{-1}), A is basin upstream contributed area of each cell (km^2), R is relative relief difference between the highest relief of the contributed basin to that cell and the elevation of that particular cell (km), and T is average temperature of the upstream contributed area (°C). The B term accounts for geological and human factors through a series of secondary equations and lookup tables, and includes the effect of glacial erosion processes (I), lithology (L) that expresses the hardness of rock, sediment trapping in reservoirs (T_E) and a human-influenced soil erosion factor (E_h) (Syvitski and Milliman, 2007):

$$B = IL(1-T_E)E_h. \tag{10}$$

The T_E and E_h parameters are temporally variable. Their value is updated during the model run from temporally explicit reservoir capacity and population density input. See Syvitski and Milliman (2007) for details regarding the *BQART* parameters and Cohen et al. (2013) for their spatially explicit implementation in the WBMsed model.

The *Psi* equation is applied to resolve the suspended sediment flux on a daily time step from the long-term sediment flux estimated by *BQART* (Eq. 9). A classic way to calculate the daily suspended sediment fluxes would be by $Qs = aQ^{1+b}$, however Morehead et al. (2003) developed the *Psi* equation such that the model is capable of capturing the intra- and inter-annual variability that can be observed in natural river systems:

$$\left(\frac{\overline{Q}_{s[i]}}{\overline{Q}_s}\right) = \psi_{[i]}\left(\frac{\overline{Q}_{[i]}}{\overline{Q}}\right)^C \tag{11}$$

where $Qs_{[i]}$ is the suspended sediment flux for each grid cell, $Q_{[i]}$ is the water discharge leaving a grid-cell, $\psi_{[i]}$ describes a lognormal random distribution, [i] refers to a daily time step, and C is a normally distributed rating exponent (Syvitski et al., 2005) with:

$$E(\psi) = 1 \tag{12a}$$

$$\sigma(\psi) = 0.763(0.99995)^{\overline{Q}} \tag{12b}$$

and

$$E(C) = 1.4 - 0.025T + 0.00013R + 0.1451n\left(\overline{Q}_s\right) \tag{12c}$$

$$\sigma(C) = 0.17 + 0.0000183\overline{Q} \tag{12d}$$

where E and σ are respectively mean and standard deviation. Eqs. (12a–12d) are reflecting the different variability behaviors of various sizes of river systems, where large rivers with high discharges tend to have less intra-annual variability in the suspended sediment flux compared to smaller systems (Morehead et al., 2003).

In WBMsed v2.0 suspended sediment reaching the floodplain reservoir will be deposited at a user defined rate. For the sake of simplicity, we assume here that all suspended sediment in the overbank flow is deposited on the floodplain. This is a reasonable assumption given that the settling velocity of silt (~0.01 mm in diameter) is about 13 m/day in clear water (Julien, 1995; Anderson and Anderson, 2010). The effect of this process is a reduction in suspended sediment flux toward the river outlet as a function of flood frequency.

2.2. Departure and continental trend analysis

Temporal changes in suspended sediment flux and water discharge are quantified by applying a normalized departure analysis technique. Departure is the difference between long-term average and a value at a grid-cell at a given time. For example, departure (D) in water discharge is

$$D_t = Q_t - \overline{Q} \tag{13}$$

where t is representing a specific point in time at a given time-scale. Here we calculate yearly departure so Q_t is the mean discharge for year t (e.g. 1960). In order to allow a dimensionless comparison between pixels and between parameters we use normalized departure

$$D_t = \frac{\left(Q_t - \overline{Q}\right)}{\overline{Q}}. \tag{14}$$

This is equivalent to the percent difference between long-term average and yearly mean.

Continental-wide departure is calculated by averaging the yearly and long-term suspended sediment and water discharge for all cells within a continent (Eq. 14). Continental-wide departure can also be calculated by averaging pixel-scale departure values. However, this approach would bias the results toward highly fluctuating pixels.

2.3. Simulation settings

For this paper, a daily 6 arc-min (~11 km) global water discharge and suspended sediment flux simulation was generated over a 50 year period, 1960–2010. The precipitation input dataset is obtained from the Global Precipitation Climate Center (GPCC), Offenbach, Germany (gpcc.dwd.de) using their "Full" product, which combines long-term precipitation climatology, derived from the entire data archive, with anomalies estimated from the operating meteorological stations at any given time. The GPCC "Full" product is available at monthly time steps at a 30 arc-minute spatial resolution. Daily partitioning of the monthly precipitation totals was established by computing the daily fraction of the monthly precipitation from the NCEP reanalysis product (Kalnay et al., 1996; Kistler et al., 2001). A six-minute topological network (Vörösmarty et al., 2000) was derived from the high-resolution gridded network HydroSHEDS using the SRTM elevation dataset (Lehner et al., 2008). These are the same datasets used in Cohen et al. (2013) and is described more comprehensively there. All datasets are available on the CSDMS High Performance Computer Cluster (http://csdms.colorado.edu/wiki/HPCC_portal). In light of the model predictive limitations for small rivers, described below, a filter was applied to mask cells with a contributing area smaller than 40,000 km^2 (based on our validation results below) and average discharge smaller than 30 m^3/s (the lower limit of the *BQART* equation).

3. Results

3.1. Model validation

The WBMsed v.2.0 model is evaluated at 10 globally distributed sites from the Global Runoff Database Center (GRDC, 2012) and 6 U.S. sites (Fig. 2; Table 1). The U.S. sites are a subset of the sites used in Cohen et al. (2013) to evaluate the first version of WBMsed. These sites are obtained from the USGS National Water Information System (NWIS) website (U.S. Geological Survey, 2012) and provide the daily suspended sediment flux and water discharge data between 1997 and 2007. Freely available, long-term observation programs of suspended sediment flux are rare outside the U.S. The 10 global sites used only provide water discharge data at different time intervals. These sites were chosen to validate river discharge as they represent wide geographical settings as well as a large spectrum of river discharges.

For the global sites (Fig. 3) WBMsed v.2.0 water discharge predictions show varying degrees of correspondence to measured discharge. The Niger, Mekong and Amazon Rivers are well predicted. The predictions in the Amazon show a lead-time of about two months (the model outsteps the observed discharge), a common issue for simulating this large river (e.g. Yamazaki et al., 2012). Model predictions for the Yellow, Danube, Ob and Amu Darya Rivers are less favorable but overall are also reasonably well corresponding to measured time series. Simulated water discharge at the Congo River is overpredicted by about a factor of 2 despite the fact that three other tropical rivers (Amazon, Niger and Mekong) are well predicted. A similar discrepancy between observed and model predicted discharge for the Congo River was reported in Arora (2001) and Yamazaki et al. (2011). Arora (2001) related the error to precipitation uncertainties. It may also be due to the location of this specific gauging station on a particularly wide section of the Congo River (near the city of Kinshasa). This demonstrates the inherent uncertainty in river gauging, particularly when multiple sources of data are used. River gauging was estimated

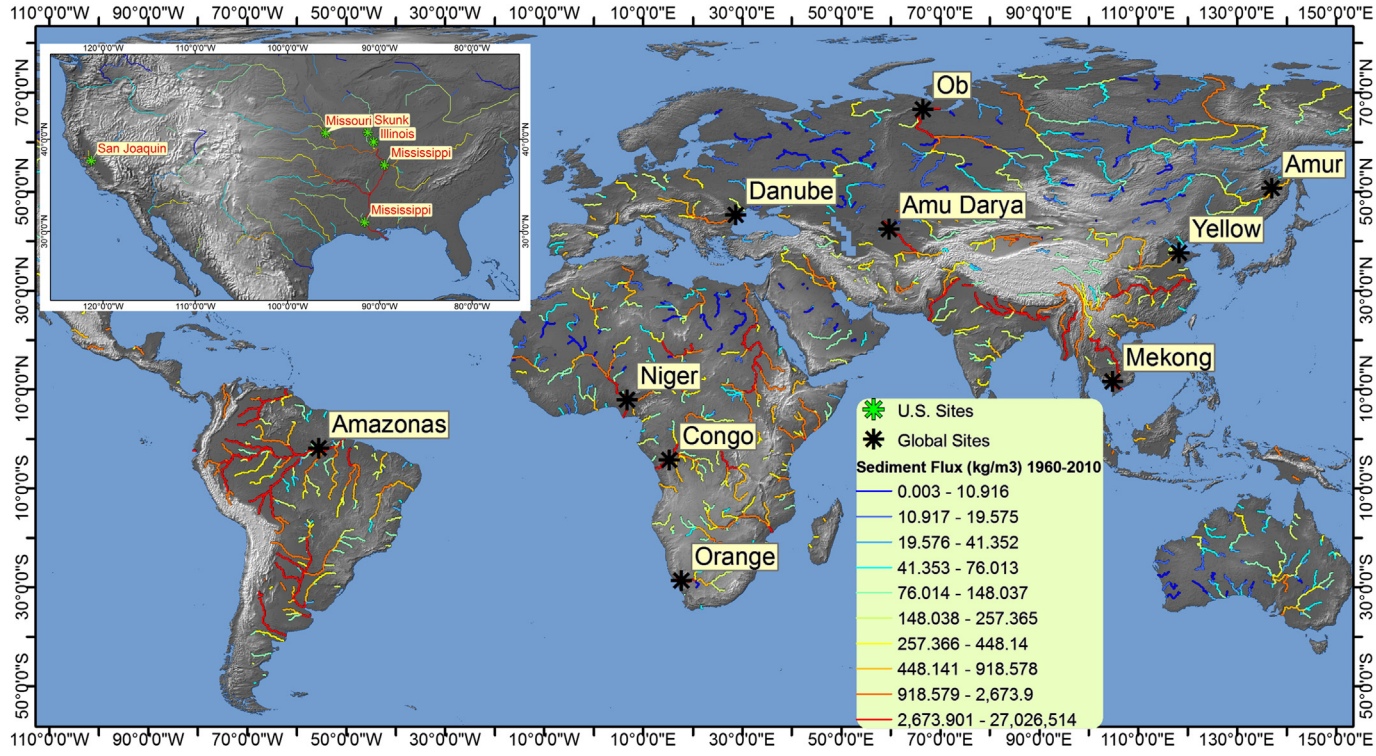

Fig. 2. Gauging stations used for validation. The U.S. stations (inner map) include both water discharge and sediment flux while global stations include only water discharge (see also Table 1). Colored rivers reflect the simulated suspended sediment flux (averaged for 1960–2010) presented here for only the larger sized river systems (drainage area >40,000 km^2, and water discharge >30 m^3/s^{-1}). (For interpretation of the references to colors in this figure legend, the reader is referred to the web version of this article.)

Table 1
Characteristics of 10 global and 6 USGS hydrological stations (Fig. 2) used to validate WBMsed simulated sediment and water fluxes. The sites' drainage area is from the gauging station metadata and the WBMsed drainage area is the model calculated contributing area for each location.

River name	Country	Coordinates lat/long (dd)	Site drainage area (km^2)	WBMsed drainage area (km^2)
Yellow	China	37.53/118.3	737 619	811 229
Amur	Russia	50.63/137.12	1 730 000	1 866 473
Niger	Nigeria	7.8/6.76	NaN	2 469 310
Danube	Romania	45.22/28.73	807 000	784 896
Ob	Russia	66.63/66.6	2 430 000	2 478 666
Congo	Congo	−4.3/15.3	3 475 000	3 640 766
Orange	South Africa	−28.76/17.73	850 530	823 111
Mekong	Cambodia	11.58/104.94	663 000	755 444
Amu Darya	Uzbekistan	42.34/59.72	450 000	670 002
Amazon	Brazil	−1.94/−55.59	4 640 300	4 683 872
Mississippi at Tarbert Landing, MS	USA	31.00/−91.62	2 913 477	3 206 630
Mississippi at Thebes, IL	USA	37.21/−89.46	1 847 179	1 841 230
Missouri at Nebraska City, NE	USA	40.68/−95.84	1 061 895	1 056 940
Illinois at Valley City, IL	USA	39.70/−90.64	69 264	69 450
Skunk at Augusta, IA	USA	40.75/−91.27	11 168	11 202
San Joaquin near Vernalis, CA	USA	37.67/−121.35	35 058	22 772

to have an error of 6–19% for water discharge and 9–53% for suspended sediment flux (Harmel et al., 2006).

The Orange River site is poorly predicted. It is likely due to the fact that it is located immediately downstream from the Vioolsdrif Dam, which was built for storing irrigation water. WBMsed includes a dam and reservoir component that estimates water release as a function of daily and mean river discharge. However, predicting the exact dam operation magnitude and schedule at a global scale is challenging, especially in dry environments where reservoir water is extensively used for irrigation.

For the U.S. sites (Fig. 4), discharge predictions by WBMsed v.2.0 correspond well to the USGS gauging data. These predictions are considerably better than those of the original model (Cohen et al., 2013), which tended to overpredict the daily peak discharge, often by orders-of-magnitude. Suspended sediment flux is overpredicted in all but two sites (Illinois and Skunk). Even so these predictions are considerably better than the original WBMsed model results where peak suspended sediment fluxes are orders-of-magnitude higher than observed fluxes (Fig. 5). The lower Mississippi site is considerably overpredicted while sediment predictions are improving upstream (the Illinois site is even underpredicted). This is because the lower Mississippi Tarbert Landing station is located downstream from the Atchafalaya River distributary, which diverts about 25% of the Mississippi River flow to the Atchafalaya River since the 1960s (Meade and Moody, 2010). The WBMsed model cannot yet simulate this kind of flow divergence.

The modeled water discharge prediction at the Skunk River site corresponds well to measured data but the predicted suspended sediment flux is considerably underestimated. This small basin (11,168 km^2) has a high density of agricultural activity. WBMsed human-influenced soil erosion factor (E_h; Eq. (10)) is a function of population density and a country's GDP (Syvitski and Milliman, 2007). This limits the effective spatial resolution of E_h in WBMsed. As a result it may under estimate agriculturally-intensive basins in developed countries as these regions, with high GDP and low population density, will yield a very low E_h. These results demonstrate the need to introduce a more sophisticated and spatially explicit human/land-use erosion factor. More explicit land-use parameterization for the *BQART* model was introduced in Kettner et al. (2010) for the Magdalena River in Colombia and in Kettner et al. (2007) for the Waipaoa River in New Zealand, however it is not yet available for a spatial distributed model like WBMsed.

Overall the model predictions correspond reasonably well to observed data. However the scope of this validation procedure is very limited. In Cohen et al. (2013) the model's long-term average sediment predictions (Eq. 9) were compared to observed data from 95 rivers worldwide ($R^2 = 0.66$). The fit between observed and predicted long-term average sediment did not significantly change in the new model version. The accuracy of the model's temporally explicit predictions was improved for the U.S. sites but remains unknown outside the U.S. The analysis in this paper therefore focuses on long-term trends and regional variability. A more comprehensive validation database is clearly needed and will be addressed in the near future.

3.2. Distributed departure analysis

Fig. 6 shows that intra-basin variability in departure can be significant. For example in the 1980s the Amazon basin had a very high departure in its southern tributaries and low departure in its middle and northern parts. The Mississippi Basin in the 1990s had a particularly high departure in its middle reaches. These kinds of variability can only be measured using a dense network of gauging stations, which is a rarity. This demonstrates one of the advantages of implementing the distributed continental model for intra-basin analysis.

Tropical rivers show relatively low inter-decadal fluctuations (i.e. neutral average departure). One clear exception is the southwestern reaches of the Amazon during the 1980s that yielded significantly above average suspended sediment (positive departure). The processes leading to this will be discussed below. Eastern Australia shows lower than average suspended sediment yield during the 1960s and 2000s, likely due to prolonged droughts during these decades. Intra-continental variability in Australia can be considerable (e.g. 1990s). Below we discuss the interplay between precipitation, water discharge and suspended sediment that can lead to these spatio-temporal dynamics.

3.3. Continental departure analysis

Figs. 7–8 show continental-average normalized departures for both sediment and water discharge at yearly time steps. Fig. 9 shows the correlation between these outcomes. These results are described for each continent below.

Asia: Two to three-year cycles of above and below average water discharge (Fig. 8) can be observed with decreasing amplitude in recent years. Suspended sediment flux also fluctuates but at one to two-year cycles (Fig. 7). The 2000s decade exhibits a decreasing trend in suspended sediment flux in contrast to discharge. This disconnection between water and sediment departure patterns is evident in their overall R^2 correlation of 0.35 (Fig. 9). The Asian departure amplitudes are the lowest of all the continents, likely due to signal averaging given the size of the landmass of this continent.

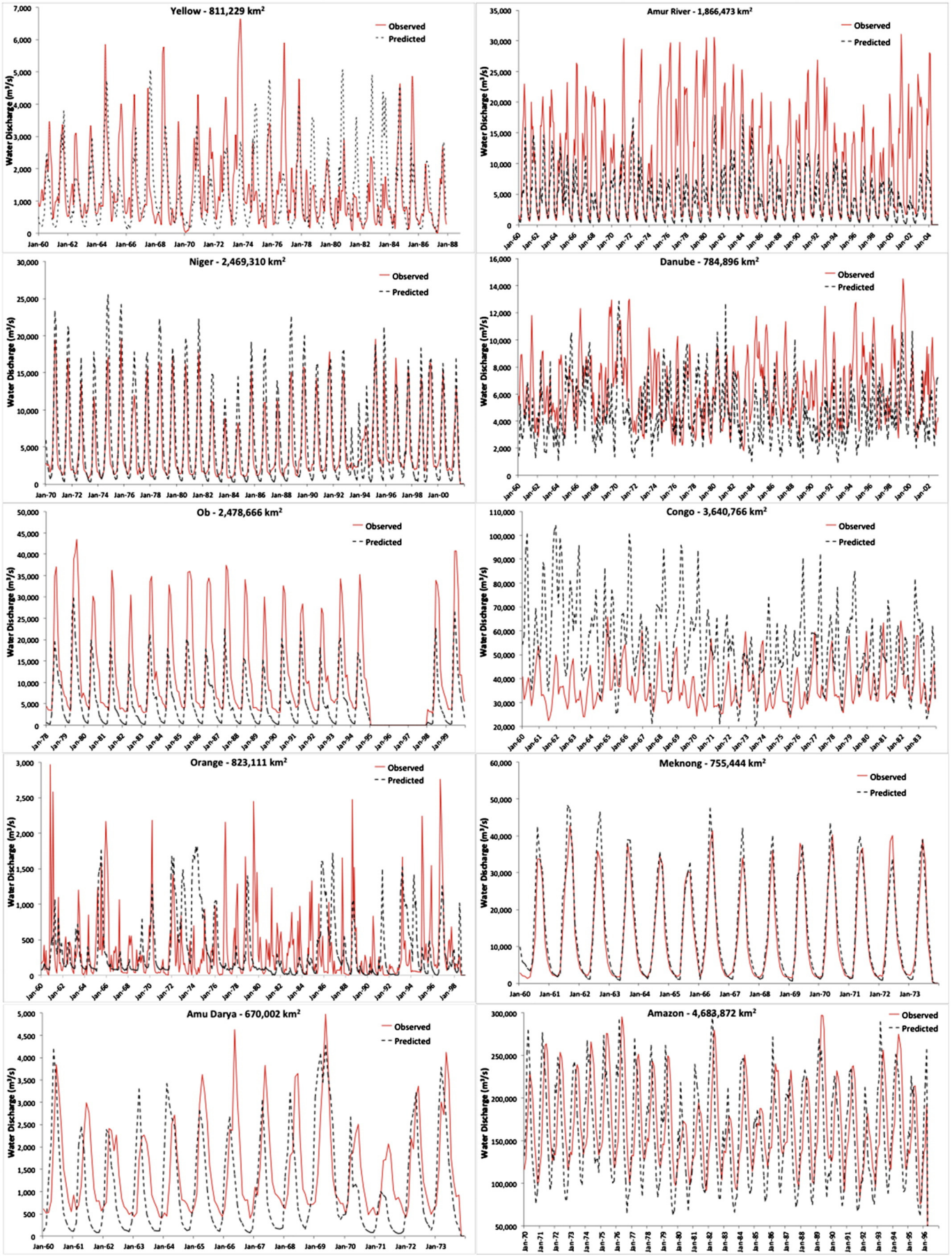

Fig. 3. Time series (monthly time steps) of observed and simulated water discharge used for validation of the globally distributed sites (Table 1 and Fig. 2).

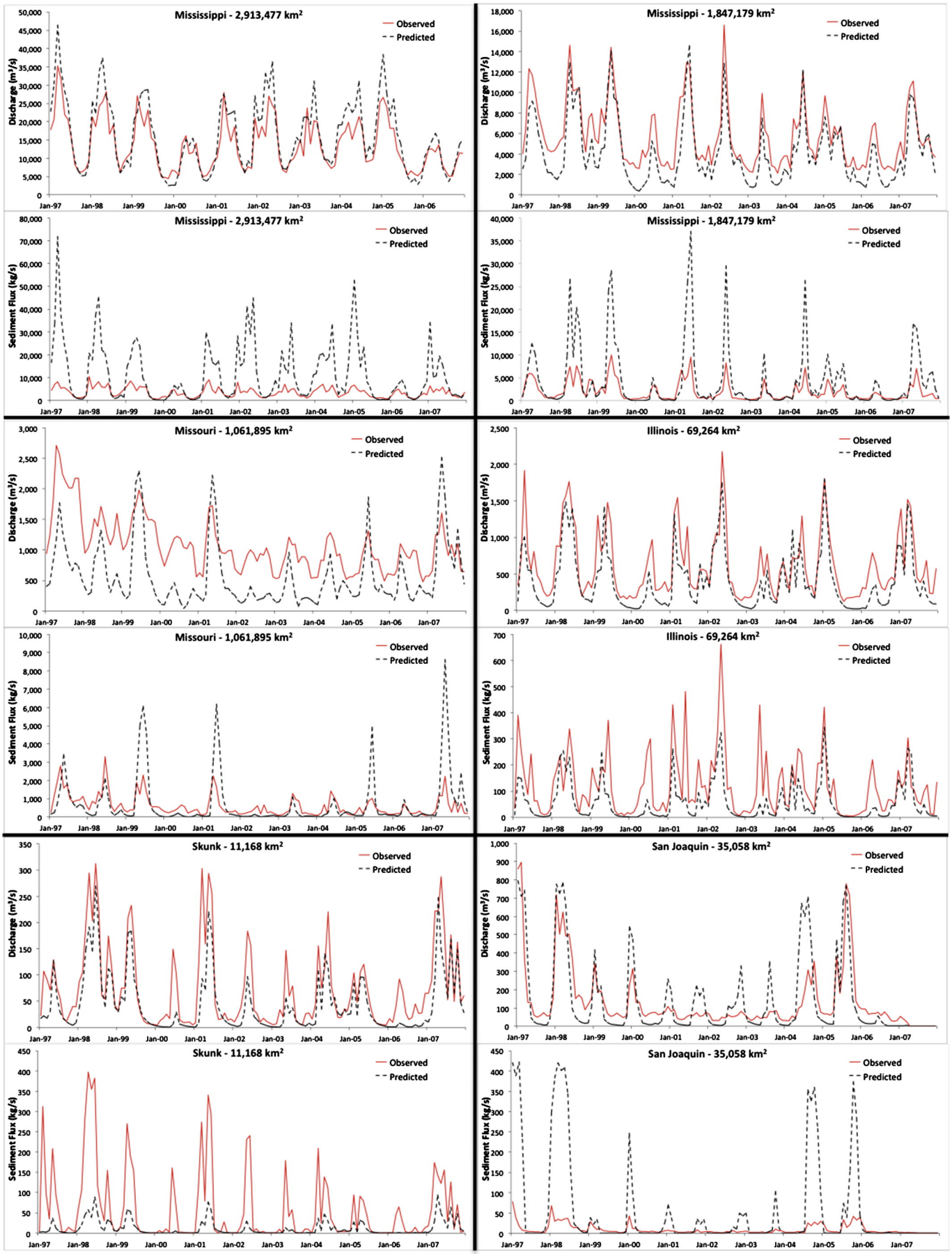

Fig. 4. Time series (monthly time steps) of observed and simulated water discharge (top plots) and sediment flux (bottom plots) used for validation of the U.S. sites (Table 1 and Fig. 2).

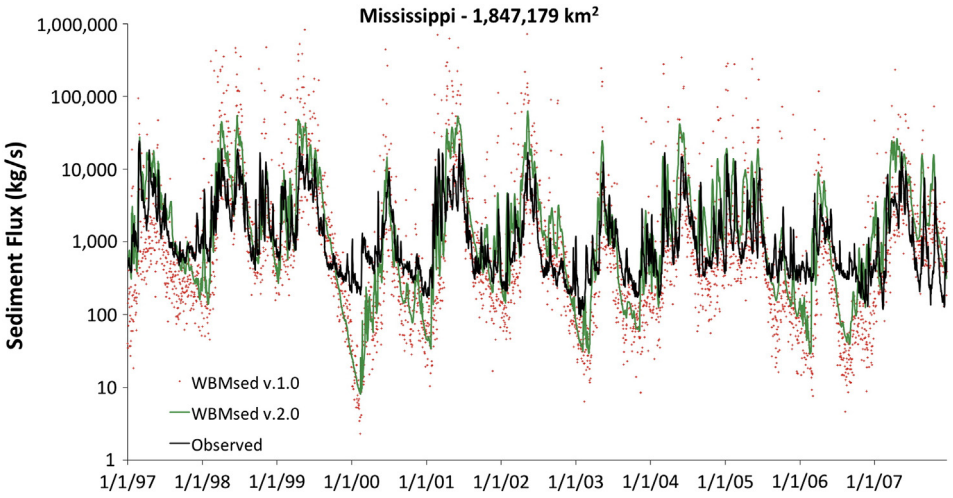

Fig. 5. Daily time series for the upper Mississippi site (Table 1 and Fig. 2) comparing the original WBMsed model (v.1.0) and the new model (v.2.0) against observed suspended sediment flux.

North America: Below average water and sediment discharge for most of the 1960s and early '70s followed by multiyear cycles of positive and negative departures with a wavelength of several years. Suspended sediment trends correspond well to water discharge ($R^2 = 0.64$; Fig. 9), however the amplitude of the sediment flux is more pronounced (maximum of >200% compared to ~50%). Overall, periods of high-suspended sediment flux are short and intense though their intensity is less in recent years.

Europe: Below average water discharge can be observed in the early 1960s followed by cycles of positive and negative departures at a wavelength of a few years, particularly after the mid 1980s. Suspended sediment departure poorly corresponds to water discharge ($R^2 = 0.24$) most notably in the 1980s and the 1990s during which sediment flux is continuously below average while water discharge fluctuates.

Africa: Above average water and sediment discharge occurred throughout the 1960s followed by relatively low amplitude cycles of negative and positive departure at a wavelength of several years. A strong correspondence exists between sediment and water discharge ($R^2 = 0.87$). The very high flows throughout the 1960s are in contrast with the other continents. This may relate to the timing of dam emplacements for the other continents. In

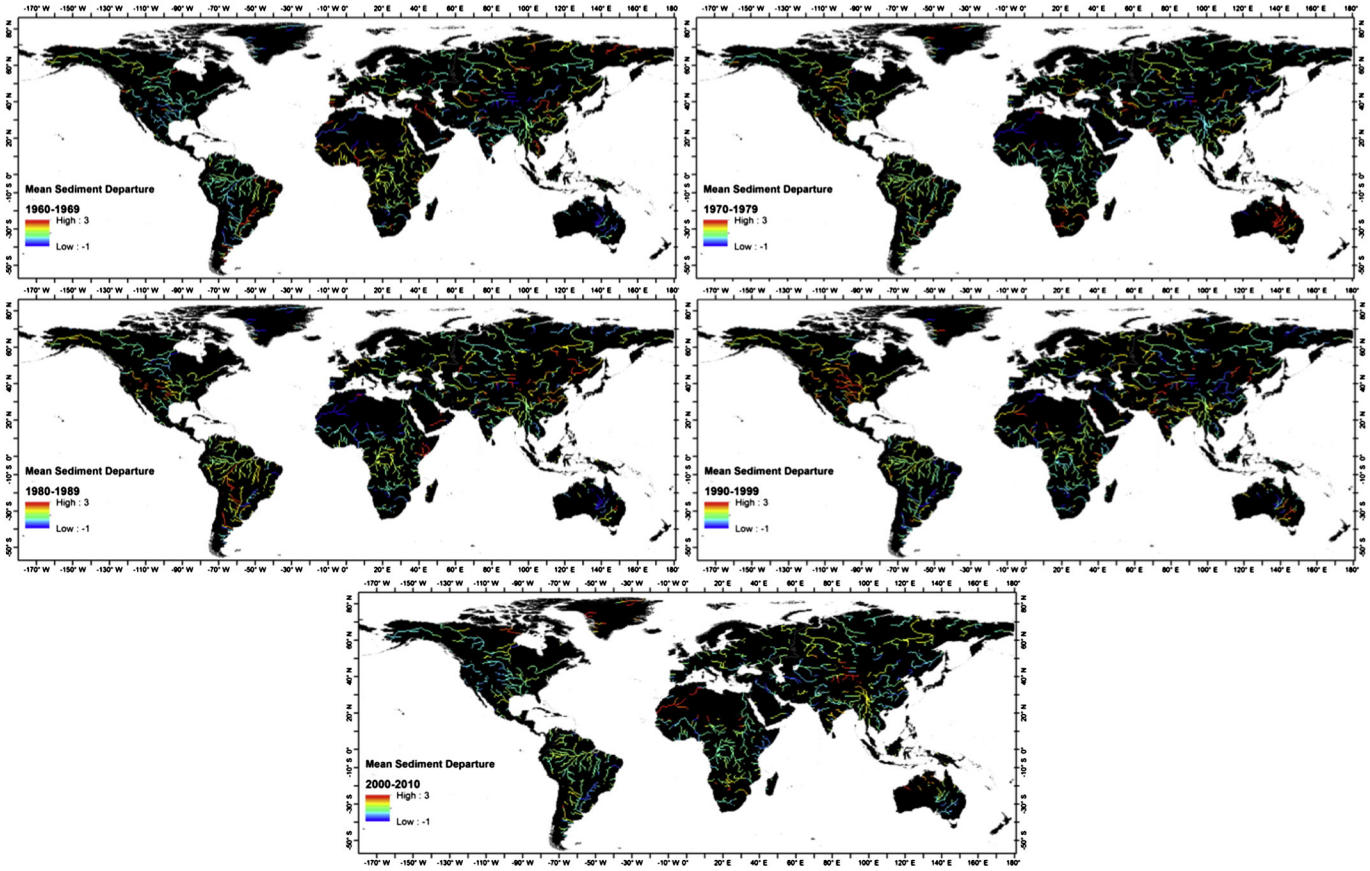

Fig. 6. Simulated decadal suspended sediment normalized departure from mean maps.

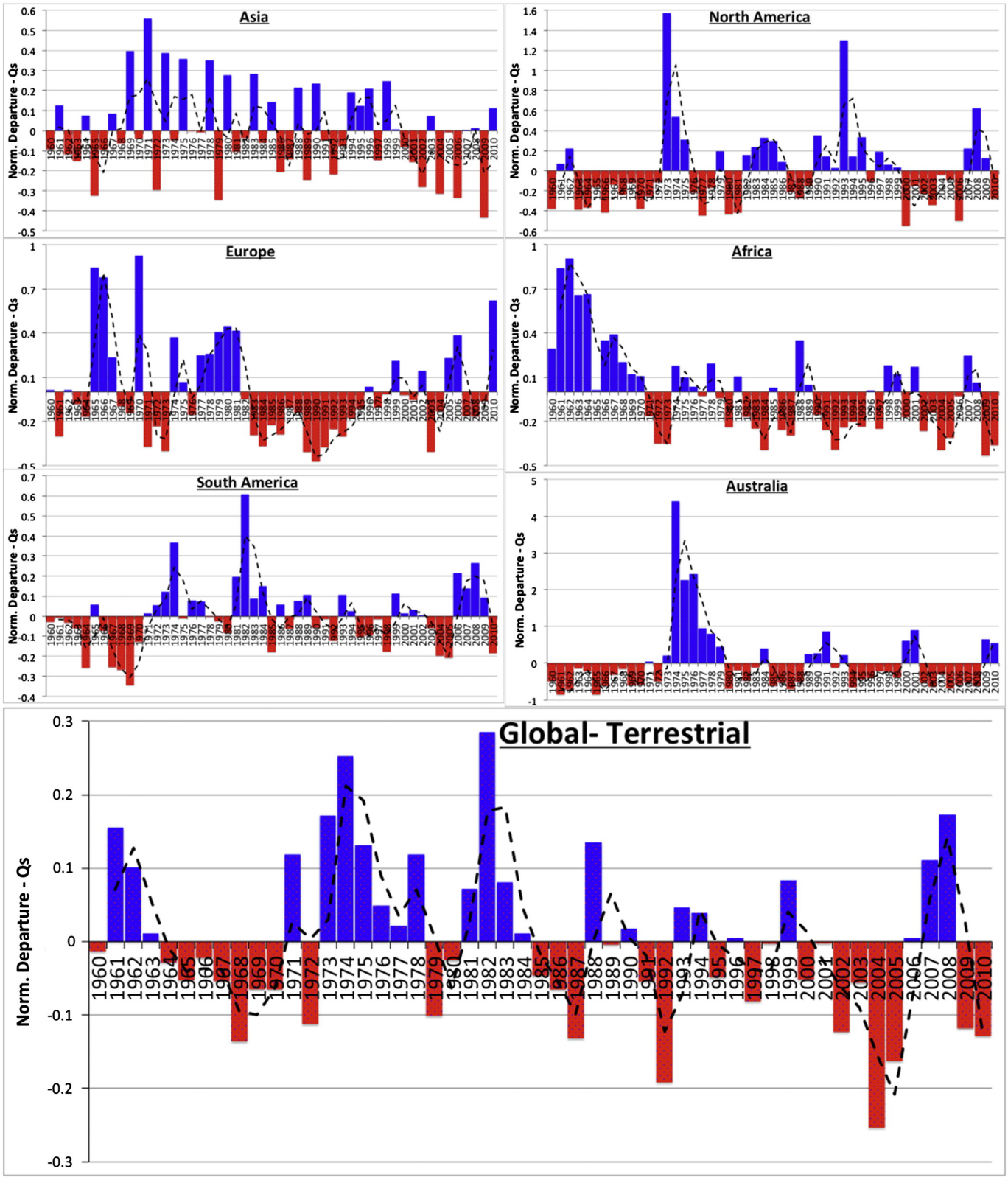

Fig. 7. Simulated average continental sediment flux normalized departure from mean plots (1960–2010).

addition to considerably reducing sediment flux downstream, dams can reduce river water discharge by evaporation and diverting flow from reservoirs for irrigation purposes. Compared to North America, Europe and Asia, large dam emplacements started overall later in Africa (1970s; World Commission on Dams, 2000).

South America: The early 1960s have a weak positive departure for water discharge and a weak negative departure for suspended sediment. Correspondence between suspended sediment and water discharge improves over time and is overall strong ($R^2 = 0.73$). Most of the 1970s show above average water and sediment discharge but

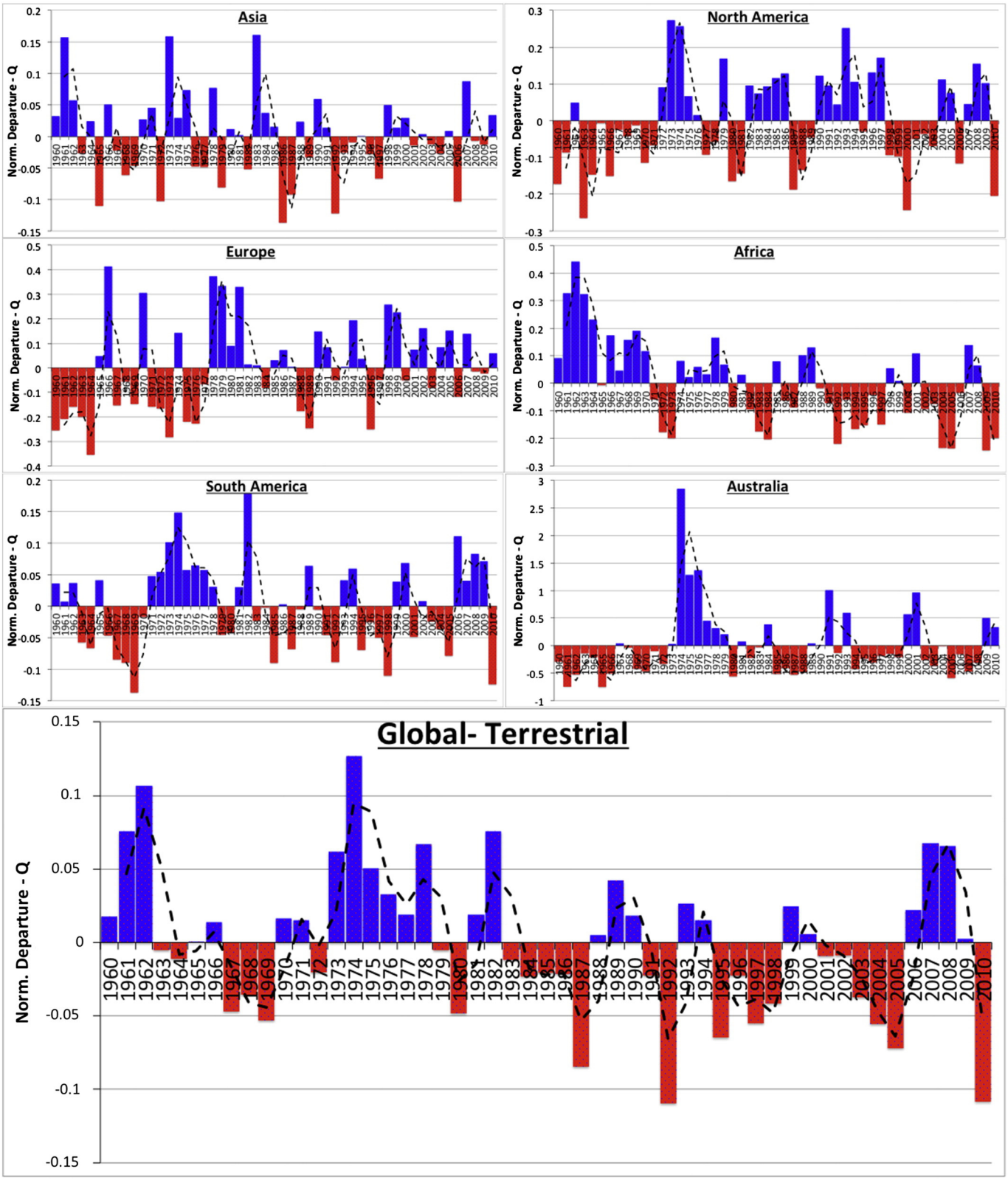

Fig. 8. Simulated average continental water discharge normalized departure from mean plots (1960–2010).

with relatively low amplitude. From the late 1970s onward, cycles of negative and positive departure have low amplitude.

Australia: A very strong correlation exists between suspended sediment and water discharge ($R^2 = 0.93$). Below-average departures occur during the 1960s and early 1970s. Very high positive departure exists during the later 1970s followed by multi-year cycles of negative and positive departures at an amplitude of several years. Below average water and sediment discharge can be observed between 2002 and

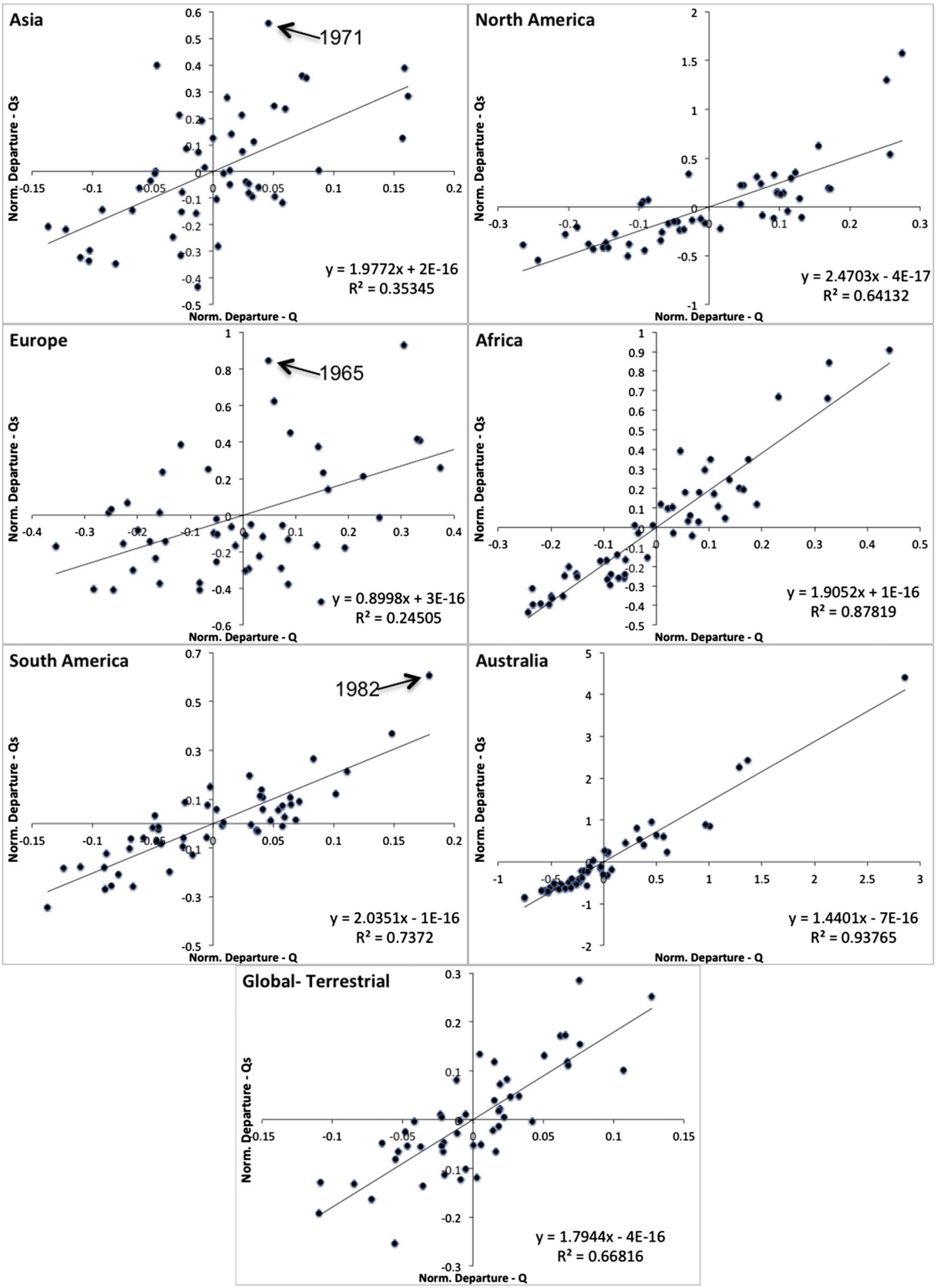

Fig. 9. Continental scatter plots between simulated sediment flux (x axis; Fig. 7) and water discharge (y axis; Fig. 8) normalized departure from mean.

2008. These very distinct cycles are likely due to persistent drought periods, which are a known climatic characteristic in parts of the Australian continent.

Global: Cycles of water and sediment discharge occur with a general trend of decreasing wavelength over time with moderate coherency ($R^2 = 0.66$).

4. Discussion

Agreement between water and suspended sediment discharge departure (Fig. 9) varies considerably between continents. The goodness of fit cannot be readily explained by the size or heterogeneity of a continent (e.g. both Asia and Europe have weak correlations) or any other clear geographical attribute. Weak correlation between water discharge and suspended sediment indicates that annual changes in water discharge explain only part of the annual fluctuations in suspended sediment, suggesting that other parameters will most likely be more dominant drivers of the temporal changes in simulated suspended sediment dynamics. These parameters likely have some degree of spatial as well as temporal variability to lead to such weak correlations. For example, dam emplacement may lead to a considerable reduction of sediment flux due to trapping (Vörösmarty et al., 2003; Syvitski and Kettner, 2011) but will not necessarily significantly reduce water discharge at a yearly time scale (Biemans et al., 2011). Even though a new dam will change the ratio between suspended sediment and water discharge (i.e. sediment concentration) the change will be mostly constant in time (from the beginning of the dam operation onward) and will therefore not significantly weaken the correlation but will only change its trend. It is therefore safe to assume that fluctuating rather than trending parameters (e.g. rainfall distribution) will lead to a weaker correlation between water discharge and suspended sediment yearly departure as calculated here.

At a basin scale, the spatial and temporal variability in precipitation may have a major effect on water discharge and sediment dynamics. For example, Syvitski and Kettner (2007) showed that the correlation between suspended sediment flux and water discharge for the Po River basin (northern Italy) changed considerably depending on the source of the sediment in the basin. Relief and lithology can act as an amplifier of precipitation patterns as intensified rainfall and snowfall in high relief areas and soft (erodible) lithology may increase sediment delivery to the river. Land-use and vegetation spatial-temporal dynamics and the location of reservoirs (Syvitski and Kettner, 2007) can also be important parameters in this context.

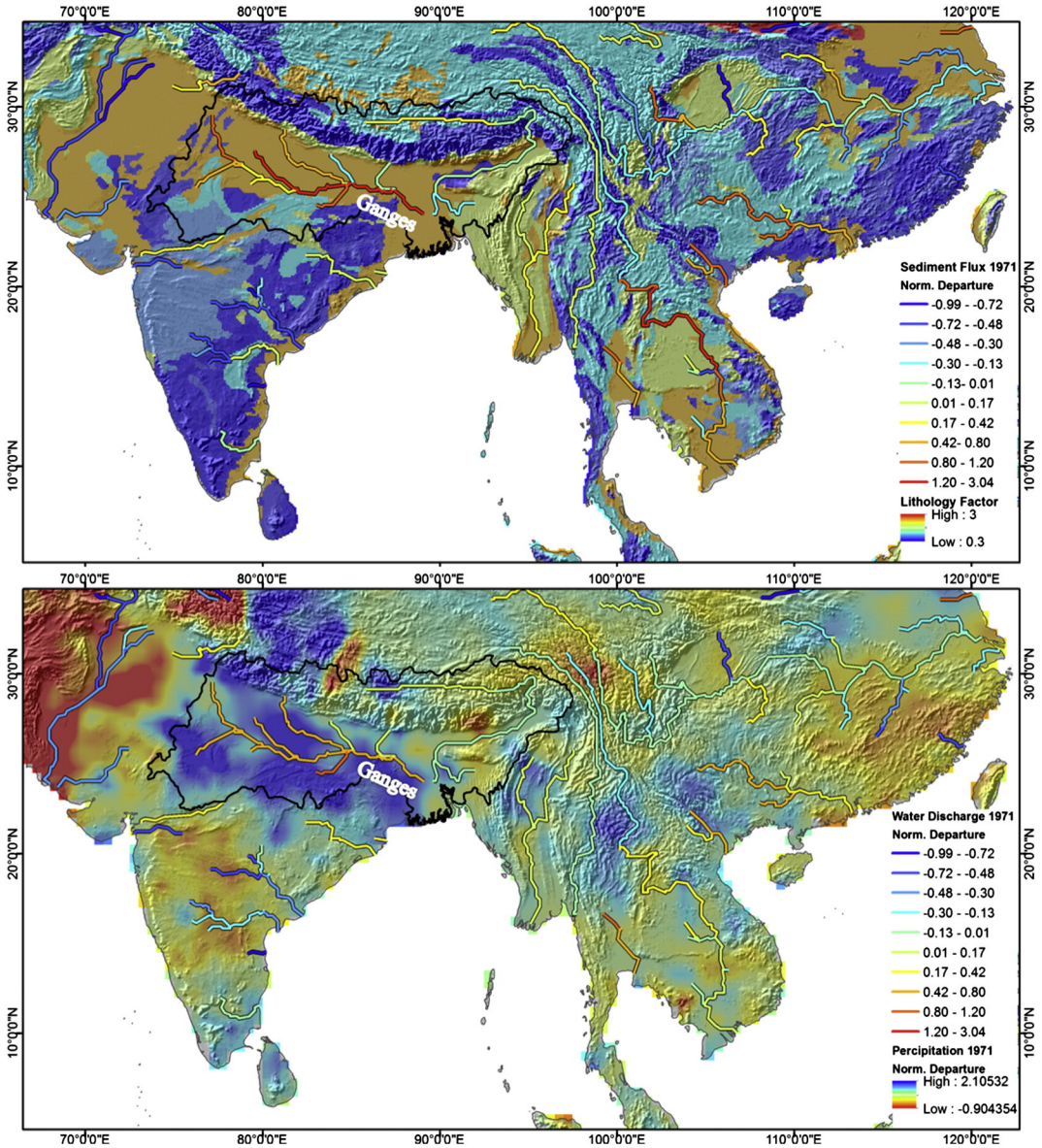

Fig. 10. Southeast Asia riverine normalized departure from mean for 1971 for: (top) sediment flux overlaying a lithology factor map, derived according to Syvitski and Milliman (2007), and (bottom) water discharge overlaying precipitation normalized departure from mean map, comparing annual precipitation of 1971 with 50 year average precipitation (1960–2010). Black line is an outline of the Ganges River Basin.

In WBMsed, human erosivity and lithology are input parameters for the *BQART* equation (E_h and L in Eq. (10)), which is used in WBMsed to simulate long-term (30+ year average) suspended sediment flux and therefore has relatively little effect on year-to-year fluctuations. Relief is a parameter in both the long-term suspended sediment equation (R in Eq. (9)) and the daily suspended sediment flux, *Psi* equation (Eqs. 11–12). We propose that intra-basin patterns of relief and lithology coupled with spatial–temporal variability in precipitation will amplify or dampen suspended sediment yield. This amplification or dampening of sediment yield results in localized (space and time) changes in the relationship between water discharge and suspended sediment, weakening the correlation at the continental level. To investigate this hypothesis we analyzed three outliers in Fig. 9 by mapping water discharge and suspended sediment departure in their respective continents and years.

For 1971, predicted suspended sediment flux in Asia was nearly 60% above average while water discharge was only 5% above average (Fig. 9). The Ganges River represents this pattern well and is therefore used here as an example (Fig. 10). The Ganges Basin received an above average precipitation that year (explaining the above average water discharge) including over the western reaches of the Himalaya range. Some parts of the Himalaya received below average precipitation resulting in lower than average water discharge in the two northeastern tributaries of the Ganges. The two northwestern tributaries show the most significant difference between suspended sediment and water discharge departure. The greatly above average suspended sediment flux in these branches of the Ganges (leading to above average suspended sediment flux at the main river stem) are the result of above average precipitation for both the Himalayans and the erosive lithology along the floodplains. The southern tributaries also received above average precipitation that year resulting in above average water discharge and suspended sediment. However since they drain significantly lower relief and less erosive lithologies, they have a better correspondence between water and suspended sediment discharge.

Simulations indicate that Europe had very high suspended sediment flux (>80% above average) in 1965 while water discharge was just slightly above average (about 5%; Fig. 9). The Danube River basin in central Europe received above average precipitation at its upper (western) reaches and below average in its lower reaches during that year (Fig. 11). A disconnect between water discharge and suspended

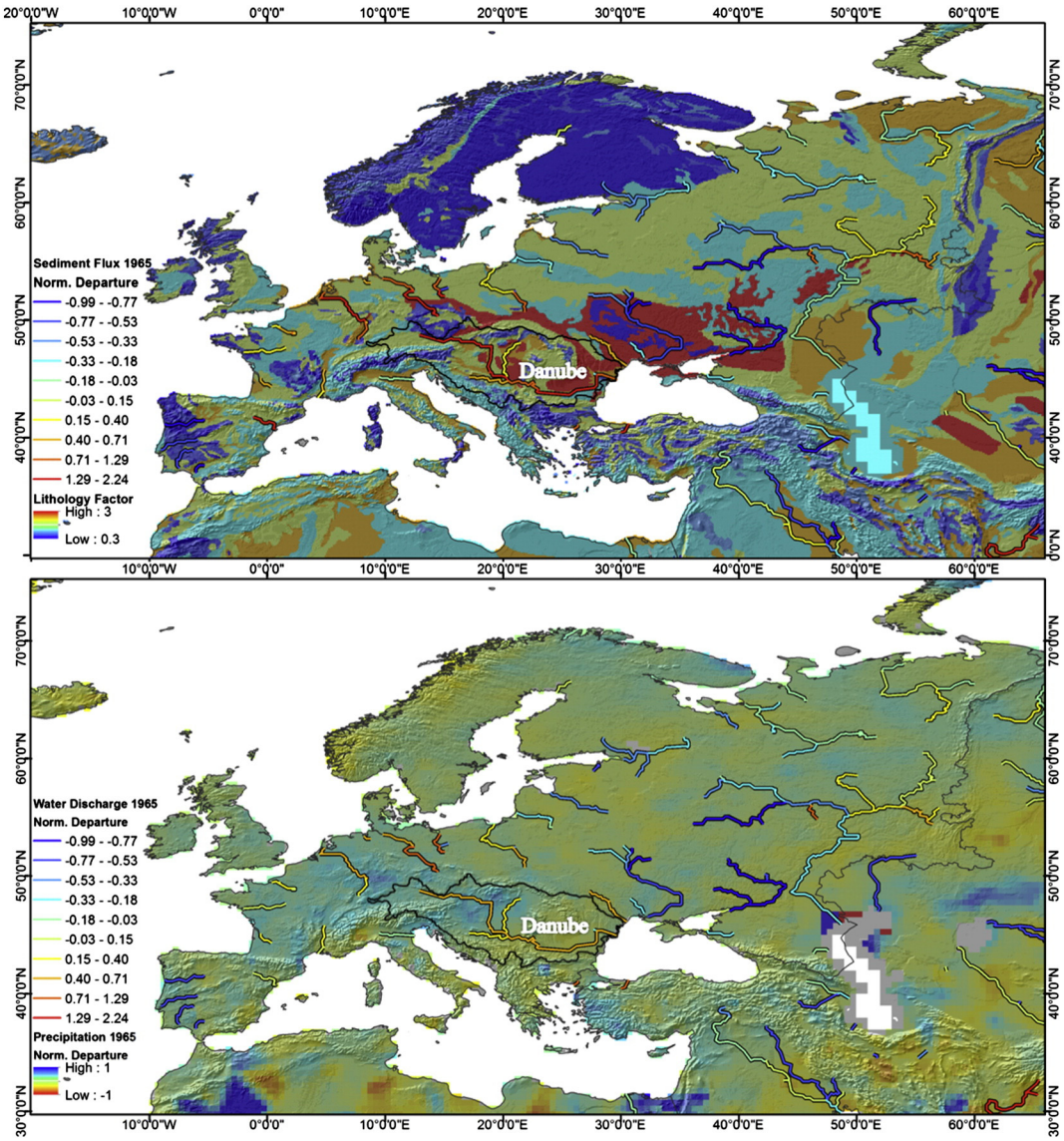

Fig. 11. Europe riverine normalized departure from mean for 1965 for: (top) sediment flux overlaying a lithology factor map, derived according to Syvitski and Milliman (2007), and (bottom) water discharge overlaying precipitation normalized departure from mean map, comparing annual precipitation of 1965 with 50 year average precipitation (1960–2010). Black line is an outline of the Danube River Basin.

sediment seems to originate at the upper reaches of the river. The lithology in this region is not particularly erosive though some patches of highly erosive (loess) lithology are included in these sub-drainage basins. The cause of the enhanced suspended sediment prediction seems to be due to the increased precipitations for the Alps and the Loess patches on the floodplain.

The last example is South America where suspended sediment flux was predicted to be about 60% above average during 1982 while water discharge predictions were less then 20% above average (Fig. 9). The *Madeira River* (the largest tributary of the Amazon River) received above average precipitation at its upper reaches (Fig. 12) resulting in above average water discharge. The *Madre de Dios* tributary yielded a considerably higher suspended sediment departure compared to its neighboring *Beni* tributary. This seems to be due to the high precipitation in its mountainous upper reaches and the lithologically erosive floodplain. The same has been predicted for the *Mamore* tributary where its east upstream branch (low relief and a mixture of high and low erosivity) received very high precipitation resulting in above average water discharge and suspended sediment while its western upstream branch (high relief and higher erosivity) yielded only moderately positive water discharge departure but high suspended sediment departure. This, again, shows that above average precipitation over high relief and erosive catchments will yield a temporary discrepancy between average sediment and water discharge.

These three examples demonstrate that the intra-basin distribution of precipitation has a substantial effect on the distribution of sediment yield. In the above analysis we only considered three degrees of freedom (precipitation, relief and lithology) however most large river systems will demonstrate more complex dynamics (e.g. land-use, vegetation, human infrastructure). This demonstrates the attractiveness of distributed numerical models as they allow us to isolate portions of these highly complex systems. This is important as future climate change is expected to have a significant effect on global precipitation dynamics (Held and Soden, 2006; Bates et al., 2008). It is therefore necessary to develop distributed predictive capabilities i.e. spatially explicit models, to enable more intelligent adaptation strategies.

5. Conclusions

In this paper we present and test a new version of the WBMsed model. The WBMsed v.2.0 model includes a floodplain reservoir component designed to simulate spatially and temporally variable storage of overbank floodwater. The model offers improved predictions of global riverine water discharge and suspended sediment flux.

We employed a normalized departure from the mean to compare yearly changes in suspended sediment and water discharge between 1960 and 2010. Results show considerable intra-basin dynamics, particularly for the more temperate regions. Tropical rivers that are responsive to the Inter-tropical Convergence Zone dynamics show relatively low temporal fluctuations. Continental average departures demonstrate a complex fluctuation pattern in suspended sediment and water discharge with a wavelength varying from over a decade to a single year. These cycles vary in time and between continents.

There appears a considerable discrepancy between water discharge and suspended sediment fluctuations for some continents (most notably Asia and Europe). We suggest that the intra-basin patterns of precipitation might enhance or dampen sediment yield as a function of relief and lithology. This explains some of the differences shown between continents as, for example, Australia (with its low relief and hard lithology) showed a very strong correlation between the fluctuation of water discharge and suspended sediment while Europe (which high relief and soft lithology regions) showed very low correlation between the two. Years with above average precipitation in high relief and soft lithology regions will yield a sediment flux that significantly exceeds increases in water discharge. This is demonstrated for the Ganges, Danube and Amazon Basins during years with high discrepancy between water discharge and suspended sediment (1971, 1965 and 1982 respectively).

Other spatially and/or temporally variable parameters will likely have a considerable effect on the sediment–discharge relationship. For example, land-use and vegetation patterns were shown to have a strong correlation to sediment yield. These parameters were not investigated here. However as future climate change is expected to significantly change precipitation, land-use and vegetation patterns, these and other

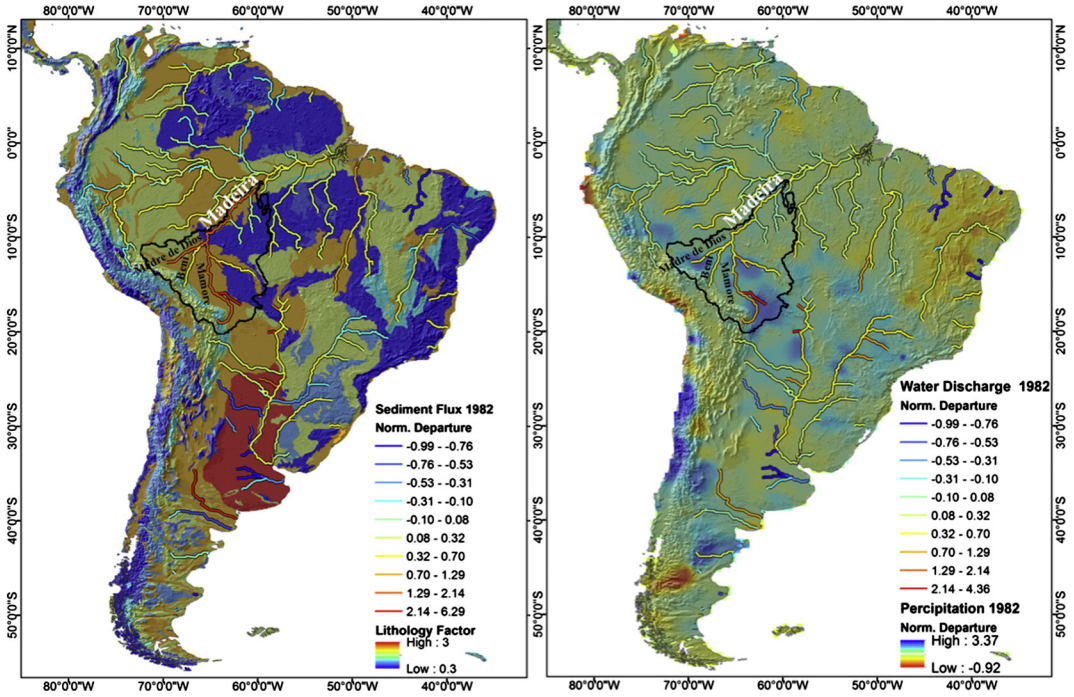

Fig. 12. South America riverine normalized departure from mean for 1982 for: (left) sediment flux overlaying a lithology factor map, derived according to Syvitski and Milliman (2007), and (right) water discharge overlaying precipitation normalized departure from mean map, comparing annual precipitation of 1982 with 50 year average precipitation (1960–2010). Black line is an outline of the Madeira River Basin.

parameters need to be considered. A systematic parametric study is therefore warranted and will be the focus of future investigations.

Acknowledgments

This research was made possible under NASA grant number PZ07124. We also gratefully acknowledge CSDMS and CU for computing time on its High-performance Computing Clusters (*Beach & Janus*). We thank Irina Overeem (UC Boulder) for her useful advices. We thank the reviewers for their very insightful and constructive comments.

References

Anderson, R.S., Anderson, S.P., 2010. Geomorphology: The Mechanics and Chemistry of Landscapes. Cambridge University Press (637 pp.).
Arora, V.K., 2001. Streamflow simulations for continental-scale river basins in a global atmospheric general circulation model. Adv. Water Resour. 24, 775–791.
Bates, B.C., Kundzewicz, Z.W., Wu, S., Palutikof, J.P. (Eds.), 2008. Climate Change and Water. Technical Paper of the Intergovernmental Panel on Climate Change, IPCC Secretariat, Geneva.
Biemans, H., Haddeland, I., Kabat, P., Ludwig, F., Hutjes, R.W.A., Heinke, J., von Bloh, W., Gerten, D., 2011. Impact of reservoirs on river discharge and irrigation water supply during the 20th century. Water Resour. Res. 47. http://dx.doi.org/10.1029/2009WR008929 (W03509).
Brakenridge, G.R., Cohen, S., de Groeve, T., Kettner, A.J., Syvitski, J.P.M., Fekete, B.M., 2012. Calibration of satellite measurements of river discharge using a global hydrology model. J. Hydrol. 475, 123–136.
Chiari, M., Friedl, K., Rickenmann, D., 2010. A one dimensional bedload transport model for steep slopes. J. Hydrol. Res. 48 (2), 152–160.
Coe, M.T., Costa, M.H., Howard, E.A., 2008. Simulating the surface waters of the Amazon River basin: impacts of new river geomorphic and flow parameterization. Hydrol. Process. 22, 2542–2553. http://dx.doi.org/10.1002/hyp.6850.
Cohen, S., Kettner, A.J., Syvitski, J.P.M., 2013. WBMsed: a distributed global-scale riverine sediment flux model — model description and validation. Comput. Geosci. http://dx.doi.org/10.1016/j.cageo.2011.08.011.
Doll, P., Fiedler, K., Zhang, J., 2009. Global-scale analysis of river flow alterations due to water withdrawals and reservoirs. Hydrol. Earth Syst. Sci. 13 (12), 2413–2432.
Fekete, B.M., Vörösmarty, C.J., 2007. The current status of global river discharge monitoring and potential new technologies complementing traditional discharge measurements. Predictions in ungauged basins: PUB kick-off. Proceedings of the PUB Kick-off meeting held in Brasilia, 20–22 November 2002. IAHS Publ., vol 309, pp. 129–136.
GRDC, 2012. The Global Runoff Data Centre. 56068 Koblenz, Germany.
Harding, R., Best, M., Blyth, E., Hagemann, S., Kabat, P., Tallaksen, L.M., Warnaars, T., Wiberg, D., Weedon, G.P., van Lanen, H., Ludwig, F., Haddeland, I., 2011. WATCH: current knowledge of the terrestrial global water cycle. J. Hydrometeorol. 12 (6), 1149–1156.
Harmel, R.D., Cooper, R.J., Slade, R.M., Haney, R.L., Arnold, J.G., 2006. Cumulative uncertainty in measured streamflow and water quality data for small watersheds. Trans. Asabe 49 (3), 689–701.
Held, I.M., Soden, B.J., 2006. Robust responses of the hydrological cycle to global warming. J. Clim. 19, 5686–5699.
Julien, P.Y., 1995. Erosion and Sedimentation. Cambridge University Press, Cambridge, UK (280 pages).
Kalnay, E., et al., 1996. The NCEP/NCAR 40-year reanalysis project. Bull. Am. Meteorol. Soc. 77 (3), 437–471.
Kettner, A.J., Syvitski, J.P.M., 2008. HydroTrend v. 3.0: a climate-driven hydrological transport model that simulates discharge and sediment load leaving a river system. Comput. Geosci. 34 (10), 1170–1183.
Kettner, A.J., Syvitski, J.P.M., 2009. Fluvial responses to perturbations in the Northern Mediterranean since the Last Glacial Maximum. Quat. Sci. Rev. http://dx.doi.org/10.1016/j.quascirev.2009.05.003.
Kettner, A.J., Gomez, B., Syvitski, J.P.M., 2007. Modeling suspended sediment discharge from the Waipaoa River system, New Zealand: the last 3000 years. Water Resour. Res. 43. http://dx.doi.org/10.1029/2006WR005570 (W07411).
Kettner, A.J., Restrepo, J.D., Syvitski, J.P.M., 2010. A spatial simulation experiment to replicate fluvial sediment fluxes within the Magdalena River, Colombia. J. Geol. 118, 363–379. http://dx.doi.org/10.1086/652659.
Kistler, R., et al., 2001. The NCEP-NCAR 50-year reanalysis: monthly means CD-ROM and documentation. Bull. Am. Meteorol. Soc. 82 (2), 247–267.
LeFavour, G., Alsdorf, D., 2005. Water slope and discharge in the Amazon River estimated using the shuttle radar topography mission digital elevation model. Geophys. Res. Lett. 32. http://dx.doi.org/10.1029/2005GL023836 (L17404).
Lehner, B., Verdin, K., Jarvis, A., 2008. New global hydrography derived from spaceborne elevation data. Eos. Trans. Amer. Geophys. Union 89 (10), 93–94.
Meade, R.H., Moody, J.A., 2010. Causes for the decline of the suspended-sediment discharge in the Mississippi River System, 1940–2007. Hydrol. Process. 24 (1), 35–49.
Morehead, M.D., Syvitski, J.P., Hutton, E.W.H., Peckham, S.D., 2003. Modeling the temporal variability in the flux of sediment from ungauged river basins. Glob. Planet. Chang. 39 (1–2), 95–110.
Paiva, R.C.D., Collischonnm, W., Tucci, C.E.M., 2011. Large scale hydrologic and hydrodynamic modeling using limited data and a GIS based approach. J. Hydrol. 406 (3–4), 170–180.
Pelletier, J.D., 2012. A spatially distributed model for the long-term suspended sediment discharge and delivery ratio of drainage basins. J. Geophys. Res. 117. http://dx.doi.org/10.1029/2011JF002129 (F02028).
Syvitski, J.P.M., Kettner, A.J., 2007. On the flux of water and sediment into the Northern Adriatic Sea. Cont. Shelf Res. 27 (3–4), 296–308.
Syvitski, J.P.M., Kettner, A.J., 2011. Sediment flux and the Anthropocene. Philos. Trans. Roy. Soc.A Math. Phys. Eng. Sci. 369 (1938), 957–975.
Syvitski, J.P.M., Milliman, J.D., 2007. Geology, geography, and humans battle for dominance over the delivery of fluvial sediment to the coastal ocean. J. Geol. 115 (1), 1–19.
Syvitski, J.P.M., Kettner, A.J., Peckham, S.D., Kao, S.J., 2005. Predicting the flux of sediment to the coastal zone: application to the Lanyang watershed, Northern Taiwan. J. Coast. Res. 21, 580–587.
U.S. Geological Survey, 2012. National Water Information System data available on the World Wide Web (Water Data for the Nation). (accessed [June 2012], at URL) http://waterdata.usgs.gov/nwis/.
Vörösmarty, C.J., Moore III, B., Grace, A.L., Gildea, M., Melillo, J.M., Peterson, B.J., Rastetter, E.B., Steudler, P.A., 1989. Continental scale models of water balance and fluvial transport: an application to South America. Glob. Biochem. Cycles 3, 241–265.
Vörösmarty, C.J., Sharma, K.P., Fekete, B.M., Copeland, A.H., Holden, J., Marble, J., Lough, J.A., 1997. The storage and aging of continental runoff in large reservoir systems of the world. Ambio 26, 210–219.
Vörösmarty, C.J., Fekete, B.M., Meybeck, M., Lammers, R.B., 2000. Geomorphometric attributes of the global system of rivers at 30-minute spatial resolution. J. Hydrol. 237 (1–2), 17–39. http://dx.doi.org/10.1016/s0022-1694(00)00282-1.
Vörösmarty, C.J., Meybeck, M., Fekete, B., Sharma, K., Green, P., Syvitski, J.P.M., 2003. Anthropogenic sediment retention: major global impact from registered river impoundments. Glob. Planet. Chang. 39 (1–2), 169–190.
Wilkinson, S.N., Prosser, I.P., Rustomji, P., Read, A.M., 2009. Modelling and testing spatially distributed sediment budgets to relate erosion processes to sediment yields. Environ. Model Softw. 24, 489–501.
Wisser, D., Fekete, B.M., Vörösmarty, C.J., Schumann, A.H., 2010. Reconstructing 20th century global hydrography: a contribution to the Global Terrestrial Network-Hydrology (GTN-H). Hydrol. Earth Syst. Sci. 14 (1), 1–24.
Wollheim, W.M., Vörösmarty, C.J., Bouwman, A.F., Green, P., Harrison, J., Linder, E., Peterson, B.J., Seitzinger, S.P., Syvitski, J.P.M., 2008. Global N removal by freshwater aquatic systems using a spatially distributed, within-basin approach. Glob. Biogeochem. Cycles 22. http://dx.doi.org/10.1029/2007GB002963 (GB2026).
World Commission on Dams, 2000. Dams and Development: A New Framework for Decision-making. Earthscan, London, UK.
Yamazaki, D., Kanae, S., Kim, H., Oki, T., 2011. A physically based description of floodplain inundation dynamics in a global river routing model. Water Resour. Res. 47. http://dx.doi.org/10.1029/2010WR009726 (W04501).
Yamazaki, D., Lee, H., Alsdorf, D.E., Dutra, E., Kim, H., Kanae, S., Oki, T., 2012. Analysis of the water level dynamics simulated by a global river model: a case study in the Amazon River. Water Resour. Res. 48. http://dx.doi.org/10.1029/2012WR011869 (W09508).